WAVE SYSTEM DIAGNOSTICS FOR NUMERICAL WAVE MODELS

Jeffrey L. Hanson
Field Research Facility, US Army Corps of Engineers, Kitty Hawk, NC, USA

Robert E. Jensen
Engineer Research and Development Center, US Army Corps of Engineers, Vicksburg, MS, USA

1. INTRODUCTION

Ocean surface wave estimates from numerical spectral wave models provide critical input to a wide variety of marine activities including operational forecasting, coastal storm protection, climate assessments, coastal and offshore structure design, search and rescue, ship routing and recreational use. As all of these applications involve the safety of human life and property, the ability to accurately assess model performance and source term behavior is of paramount importance. This poses a significant challenge to model developers, as available ground truth or "benchmark" data, typically from buoys and satellite sensors, are sparse in either space or time, respectively. Furthermore, wave model validation is typically accomplished using the limited amount of information contained in mean or "bulk" wave parameters, obtained from integral properties of the spectrum (see for example Cardone et al. 1996, Hsu et al. 2002, O'Reilly et al. 1996, and Tolman 2002). As these quantities represent averages over all existing wave systems, they provide only a general measure of total model performance and can potentially mask higher order deficiencies.

Clearly the bulk validation approach does not make full use of all available information, as directional wave spectra contain valuable details on all the individual wind sea and swell wave components present in the observation or modeling domain. Furthermore, the time evolution of these wave component attributes has the potential to provide an even deeper level of diagnostics for model improvement by tracking the evolution of specific swell systems from localized generation events. Here we demonstrate the use of such wave system-level validations on a basin-scale Pacific Ocean hindcast in preparation by the US Army Corps of Engineers (USACE) Wave Information Study (WIS) program (Tracy et al. (in prep)). The results reveal that application of these techniques provide an elevated level of diagnostic information on model performance as well as important information on source term behavior.

The verification of wave model output at the wave system level requires an efficient approach to characterize energy levels of individual wind-sea and swell wave components in directional wave spectra. Here a 'wave component' is defined as a specific wind-sea or swell that can be attributed to a region of enhanced energy in the directional wave spectrum. The time evolution of a series of related wave components forms a 'wave system' that can be traced to a specific generation region on the ocean surface. Wave spectral partitioning methods have been applied in a variety of investigations, including the comparison of wave fields from the Labrador Sea Extreme Waves Experiment (Beal 1989), the validation of WAve Model WAM performance against ERS-1 SAR spectra (Hasselmann et al. 1994), the assimilation of wave observations into the WAM model (Voorrips et al. 1997), the analysis of wind sea growth and dissipation in the open ocean (Hanson and Phillips 1999), a study of swell evolution across the Pacific (Hanson and Phillips 2001), and an analysis of nearshore wave climatology (Scott et al. 2002).

Originally proposed by Gerling (1992), wave partitioning allows the identification and grouping of component wave systems from spatially and temporally distributed observations of directional wave spectra. A primary limitation to the Gerling approach is that only those portions of the spectrum that rise above a constant threshold are used to determine the features of particular wave component. Hasselmann et al. (1994) improved on this method by dividing the spectrum into subset domains based on an inverted catchment area approach, thus using the entire spectral region of each peak to compute wave component parameters. Hanson (1996) and Hanson and Phillips (2001) made further improvements to the technique by adding clustering routines to track the evolution of individual wave components and dispersion calculations to estimate the source time and location of resulting wave systems. Work has continued on the development of these techniques since the publication of Hanson and Phillips (2001), to the point that we now have a fully automated, GUI-driven system employing modern image processing technology for performing a wide range of wave system analyses on time-evolving series of directional wave spectra.

The application of wave spectral partitioning techniques to wave model verification provides a significant advantage over the use of bulk spectral parameters. Although Beal (1989) and Hasselmann et al. (1994) compared wave model output to buoy and satellite observations at the wave system level, the results are only qualitative in nature and lacked specific use of metrics for evaluating model performance. Here it is shown that the use of wave component metrics provides a unique forensics capability for diagnosing model weaknesses in the details down to the source term behavior. We demonstrate this capability on a 1-year WAM Pacific Ocean hindcast for the year 2000, using as input National Centers for Environmental Prediction-National Center for Atmospheric Research (NCEP-NCAR) global reanalysis (NRA) surface marine wind fields (Kalnay et al. 1996) that have been kinematically adjusted (Swail and Cox 2000) by *Oceanweather, Inc*. (OWI). The result is a quantification of model performance in estimating the wave height, period, and direction attributes of the specific wind-sea and swell wave components measured at several directional wave-buoy stations. Furthermore, we analyze the ability of the model to capture the life history of evolving swell systems from various storm sources in the North Pacific and Southern Hemisphere. The forensic results from these validations will be used to guide model improvements and determine the appropriate methodology to use for long-tem wave hindcasts.

2. OBSERVATIONS AND HINDCAST MODELING

2.1. Ground Truth Observations

The wave system verification method requires both wind observations and directional (2D) wave spectra as input. Ground truth data were obtained from the National Buoy Data Center (NDBC) and Coastal Data Information Program (CDIP) buoy networks. The six stations used in this study are identified in Table 1. Included are all available NDBC directional wave stations and a single CDIP station (071). The remaining CDIP buoys available during 2000 were either in partially sheltered locations or shallow depths and not ideal for validating a basin-scale wave model.

The NDBC stations provide hourly 8-min average wind speed and direction at a sensor height of 5-m above sea level. Measurement accuracy is ± 1.0 m/s for wind speed and ± 10 deg for wind direction. There is no wind sensor at CDIP station 071, however, winds from NDBC station 46063, located 23 km southeast of 071, were used to estimate local wind-generated forcing around CDIP station 071. Wind information is only used in this study to provide general guidance for locating wind-sea peaks in the directional wave spectrum. As such, the errors inherent with a short wind averaging period, low anemometer height and a spatial separation between wind and wave observations (at 071) are easily tolerated by the analysis (see section 3).

Directional wave spectra from the NDBC 2D stations are computed hourly from 20-minute records over a frequency ban of 0.03 to 0.4 Hz. Reported quantities include the non-directional (1D) energy-frequency spectrum $E(f)$, the vector mean direction $\overline{\theta}(f)$ at each frequency bin, and the directional distribution parameters $r_1(f)$, $r_2(f)$, $\alpha_1(f)$ and $\alpha_2(f)$. These quantities incorporate various corrections for hull-mooring response (Steele et al. 1992) and can be described in terms of the Longuet-Higgins fourier coefficients a_1, a_2, b_1 and b_2 as:

$$
\begin{aligned}
r_1 &= \frac{\sqrt{a_1^2 + b_1^2}}{a_\circ} \\
r_2 &= \frac{\sqrt{a_2^2 + b_2^2}}{a_\circ} \\
\alpha_1 &= 270 - \tan^{-1}\left(b_1/a_1\right) \\
\alpha_2 &= 270 - \frac{\tan^{-1}\left(b_2/a_2\right)}{2} + \{0 \ , \ 180\}
\end{aligned}
\qquad (1)
$$

where $a_\circ = E(f)$. The NDBC World-Wide Web (WWW) site (http://www.ndbc.noaa.gov/) states their wave measurement accuracies to be ± 0.2 m in wave height, ± 1.0 s in wave period, and ± 10 deg in wave direction.

The CDIP directional wave data are computed from half-hour records over the frequency band 0.025 – 0.58 Hz. Reported quantities include $E(f)$, $\overline{\theta}(f)$ and the Fourier coefficients a_1, a_2, b_1 and b_2. Stated accuracies of the Datawell directional wave buoy are 3% of buoy heave and 0.4-2 deg in direction.

The maximum-likelihood estimator of Oltman-Shay and Guza (1984) is used to compute the directional wave spectrum $S(f,\theta)$ from the NDBC and CDIP spectral parameters. The resulting spectra are linearly interpolated to the 25-frequency, 15-deg resolution of the hindcast spectra (see below). As will be shown, this step is necessary to make one-to-one comparisons between buoy and hindcast spectral features.

Table 1. Observation Stations

Organization	Station ID	Platform	Payload	Data Used	Depth (m)	Latitude	Longitude	Location
NDBC	46041	3-m discus	DACT	Met, 2D Waves	132	47°20'24" N	124°45'00" W	Cape Elizabeth, WA
NDBC	46029	3-m discus	DACT	Met, 2D Waves	128	46°07'00" N	124°30'36" W	Columbia River Bar
NDBC	46042	3-m discus	DACT	Met, 2D Waves	1920	36°45'11" N	122° 25'21"W	Monterey, CA
CDIP	00071	0.9-m sphere	Datawell MK II	2D Waves	549	34°27'00" N	120°46'48" W	Harvest, CA
NDBC	46063	6-m Nomad	DACT	Met	598	34°16'35" N	120°39'53" W	Pt. Conception, CA
NDBC	51028	3-m discus	ARES	Met, 2D Waves	4755	00°01'12" N	153°52'12" W	Christmas Island

2.2. Hindcast Wind Fields

The quality of input wind fields is of major importance in wave estimation accuracy (Cardone et al. 1995). Of several competing approaches, Cardone et al. demonstrate that the interactive objective kinematic analysis of Cox et al. (1995) produces superior wind fields for numerical wave modeling. Applying these techniques to standard Weather Prediction Center surface marine wind fields (e.g., NRA), Swail and Cox (2000) achieve a wave height bias reduction from -0.18 to -0.04 m over a 4-month hindcast period in the North Atlantic using the OWI 3-G model.

A primary goal for the USACE WIS Pacific Ocean hindcast is to develop an accurate wave climatology, from extreme storm-system related waves to everyday conditions. To achieve this goal, emphasis is placed on the development of a high quality, consistent set of wind fields. The WIS wind fields are generated by the marine meteorology group at OWI using baseline NRA 6-hourly 10-m surface winds on a Gaussian geographic grid. The NRA fields are adjusted using QuickSCAT (Q/S) scatterometer winds by linear regressions through quantile-quantile (Q-Q) plots in 45-deg wind direction sectors grouped in six 10-degree latitude bins from about 180-deg W to just off the West Coast. Wind field estimates west of 180-deg W mirror the eastern corrections to the Asian coast. Southern Hemisphere points are not adjusted. A three-grid-point buffer between adjustments at coastal points and at zonal boundaries is used to blend regions. Additional coastal corrections are made point by point. Wind direction bias is removed using mean sector differences. NRA data from the full year (2000) are included in the Q-Q analysis, as seasonally stratified regressions are not statistically independent. Besides the Q/S adjustments, no additional observations are used in the analysis of the NRA-QuickSCAT (NRAQ) winds. Compared to the NRA winds, the NRAQ winds do a superior job in capturing synoptic and meso-scale events.

At this point, a third level of analysis is performed using manual kinematic techniques for top ranked storms in each geographic region. This is necessary as hindcasts using the NRA winds are found to underestimate systematically the storm peaks (Swail and Cox 2000). All available information from buoys, ship reports and C-MAN stations are re-assimilated into the Level III analysis. The resulting NRAQ Level III fields are interpolated to 1-hour resolution on a 1-degree spatial hindcast grid. An example NRAQ Level III wind speed field used in this study appears in Fig. 1. Included in Fig. 1 are the locations of the five directional wave-buoy stations (Table 1). Note that during the November time period there are elevated wind events in both the southern and northern hemispheres that can influence wave conditions at our study sites. This will be discussed further in Section 4b.

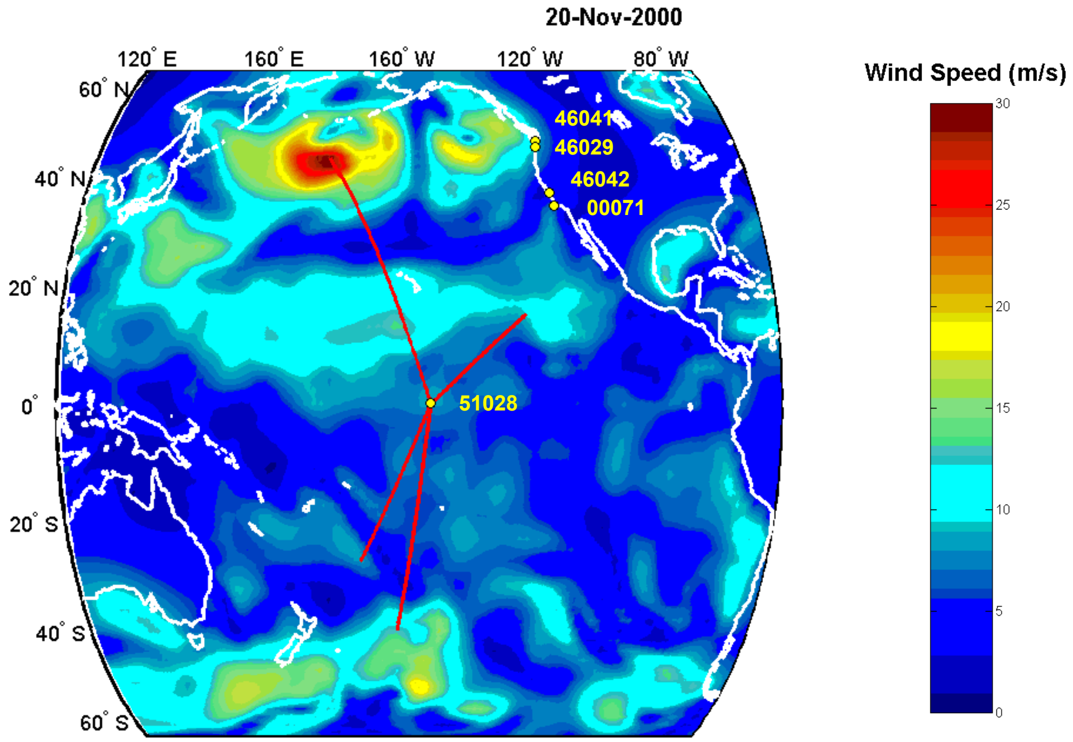

Fig. 1. Example NRAQ Level III wind field for 0200 GMT on 20 November 2000. Also indicated are the five directional wave buoy stations used in this study. Wave propagation routes (A through D) from four primary wave generation areas for station 51028 in November are shown (see section 4b for discussion).

2.3. Hindcast Wave Modeling

Numerical wave models solve the action balance equation:

$$\frac{\partial N}{\partial t} + \overrightarrow{C_g} \cdot \nabla N = \sum_{i=1}^{n} S_i \ , \tag{2}$$

where the action density N is $E(\omega)\,/\,\omega$, radian frequency $\omega = 2\pi f$, and $\overrightarrow{C_g}$ is the vector wave group velocity. The source terms on the right hand side are given by

$$S_{total} = S_{in} + S_{nl} + S_{ds}\ , \tag{3}$$

with source mechanisms grouped into a wind input term (S_{in}), nonlinear wave-wave interaction term (S_{nl}), and a dissipation term (S_{ds}). The momentum transferred to waves and currents by the winds is captured by S_{in}. The spectral shift of energy away from the peak to high and low frequencies is described by S_{nl}. For open ocean deep-water wave propagation, the primary S_{ds} mechanism is due to breaking waves. In the third generation WAM Cycle 4 (Komen et al. 1994), all source terms are specified with degrees of freedom equal to those of resulting directional wave spectra, with no *a-priori* assumptions regarding spectral shapes. WAM solves equation (2) in two parts: (a) the time-invariant propagation of energy on a fixed grid, and (b) the temporal change of action that is effected by the source terms of equation (3). Internal time steps and output resolution control model run times in time and space. Increased computing demands, necessitated by higher grid resolution, nested domains, and increased spectral resolution, have resulted in the transition of WAM Cycle 4 to a parallel processing architecture (Jensen et al. 2002).

To assess the quality of our input winds, optimize spectral resolutions, and forensically evaluate source term performance, two 12-month WAM Pacific hindcasts were produced using the NRAQ Level III winds for year 2000. The latest version of WAM (Cycle 4.5) was run on a Cray X1 platform with no parallelization. The modeling domain consisted of 19,127 active water points at 1-deg spatial resolution covering 64 S to 64 N Latitude and 110 E to 60 W Longitude. Water depths were obtained from General Bathymetric Chart of the Oceans (GEBCO), a digital bathymetry database with nominal resolution of 3-minutes. Depth data were then sub-sampled to a 1.0-deg fixed longitude, latitude grid, and edited to include spatially unresolved islands. A 1200-s internal time step was used for both temporal and spatial calculations, with output exported hourly. Full directional wave spectra were saved at 23 points, corresponding to the locations of available Pacific wave buoys (1D and 2D), including the 2D buoys listed in Table 1. Spectra were computed over 25 logarithmically spread frequencies, and 24 evenly spaced directions at 15-deg intervals. The model was initiated on January 1, 2000, and results from the first 2 'spin-up' weeks of January were not included in the analysis. Although the hindcast results were validated at all 23 NDBC sites using non-directional bulk statistics, our focus here is to explore new wave-system level validations. For this approach, we focus on data from the 2D buoy sites listed in Table 1.

3. WAVE SYSTEM ANALYSIS APPROACH

The approach to quantifying WAM performance in hindcasting the production and evolution of specific wave systems is accomplished in two separate analysis pathways using three distinct data processing modules. As outlined in Fig. 2, a wave component analysis pathway (solid red) makes use of a Spectral Partitioning Module for pre-processing buoy data, which separates the observed 2D spectra into various wind-sea and swell spectral regions or partitions. This information is passed, along with the hindcast spectra, to the Wave Component Module for determination of the differences between buoy data and wind-sea and swell component estimates. A wave system analysis pathway (dashed blue) uses the Spectral Partitioning Module to isolate the time-evolving wave components from both the observed and hindcast sets of spectra. The resulting wind-sea and swell event series are passed to the Wave System Module, which performs a diagnostic match-up of the observed and hindcast wave systems to isolate potential model deficiencies where the two differ. Detailed descriptions of the three data processing modules follow.

3.1. Spectral Partitioning Module

The basic approach to our wave spectral partitioning method is described by Hanson (1996) and Hanson and Phillips (2001), the latter hereinafter referred to as HP01. Written entirely using MATLAB®, the ocean surface wave analysis tools in the Spectral Partitioning Module were originally developed by The Johns Hopkins University Applied Physics Laboratory (JHU/APL). For completeness, we summarize the methods here and provide detail on the improvements that have been made since HP01.

a. Wave Component Identification

The first step of spectral partitioning is to isolate spectral regions $S(f,\theta)$ associated with individual energy peaks. This was accomplished by HP01 with a time-consuming recursive algorithm that assigned each spectrum value to a path of steepest ascent associated with a local peak. All paths leading to the same peak were assigned to a distinct spectral partition. This step has been improved with efficient image processing routines that were designed for making watershed delineations in topographic imagery (Soille 1999, Vincent and Soille 1991). Treating the spectrum as an inverse topographic domain, an 8-point connected smoothing transform[*] removes fine-scale noise in the spectrum. A watershed delineation transform[**] then identifies the boundaries forming the minima between remaining spectral peaks. Spectral regions surrounded by such boundaries become individual partitions. This change in basic methodology has reduced by an order of magnitude the time required to process each record, with essentially no change in output results.

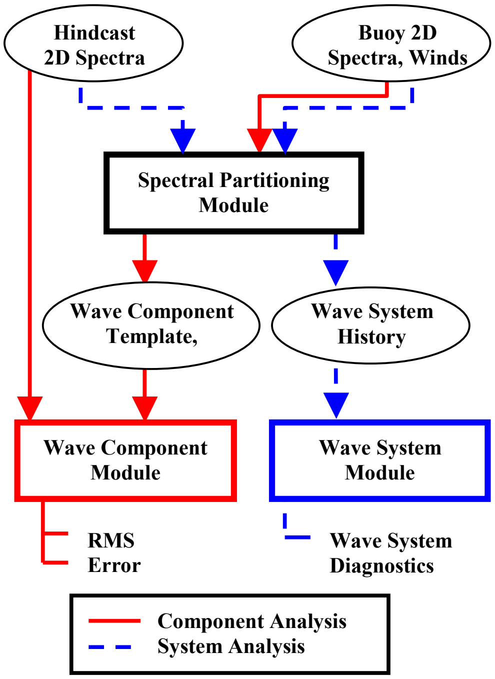

Fig. 2. Overview of wave model validation approach. See text for detailed description of how data are processing by each module.

---

[*] MATLAB® Image Processing Toolbox function imhmax.m

[**] MATLAB® Image Processing Toolbox function watershed.m

b. Wave Component Statistics

Once the initial partitions are identified, a variety of component statistics are computed to aid with further processing. These include the 1D energy spectrum

$$E(f) = \int S(f,\theta)d\theta\,;$$

the total energy in the 2D spectral domain

$$e = \int\int S(f,\theta)d\theta df\,;$$

the significant wave height, approximated by H_{mo}

$$H_s \approx H_{mo} = 4\sqrt{e}\,;$$

and the peak wave period

$$T_p = \frac{1}{f_p}\,;$$

with the peak wave frequency f_p computed from a 3-point parabolic fit to the 1D spectral peak. Also computed is the vector mean wave direction

$$\bar{\theta} = \tan^{-1}\left(\frac{\overline{\sin\theta}}{\overline{\cos\theta}}\right),$$

where

$$\overline{\sin\theta} = \frac{\int\int S(f,\theta)\sin\theta\, d\theta\, df}{e}$$

$$\overline{\cos\theta} = \frac{\int\int S(f,\theta)\cos\theta\, d\theta\, df}{e}\,;$$

and the directional spread (O'Rielly et al. 1996)

$$\sigma = \left[2(1-m_1)\right]^{1/2}\,,$$

where

$$m_1 = \left[\left(a_1^b\right)^2 + \left(b_1^b\right)^2\right]^{1/2},$$

with the bulk Fourier coefficients

$$a_1^b = \frac{1}{e}\int_{f1}^{f2} a_1(f)E(f)df$$

$$b_1^b = \frac{1}{e}\int_{f1}^{f2} b_1(f)E(f)df\,.$$

Both full spectrum and spectral component statistics are computed using the above relationships. Integration domains are implied to be over all frequency bins and from 0 to 2π in direction. For computing statistics of a spectral component, all spectral values not falling within the partition domain are set to zero.

c. Wind-sea and swell combinations

The resulting wave components are sorted into wind-sea or swell. To be classified as wind-sea, a spectral peak must be forced by a component of the existing wind. A wave-age criterion is used to identify and combine the 2D wind-sea partitions. All remaining peaks are labeled as swell. Adjacent 2D swell peaks that are contiguous in frequency can be part of the same swell system and are combined under certain conditions. Two tests are made to determine if adjacent swell peaks belong to the same wave system. A swell angle threshold test requires the mean directions of adjacent peaks be separated by less than a threshold angle. A threshold value of 30 deg yielded optimum results with the Pacific Ocean data and provided a comfortable margin outside the stated ±10-deg accuracy of the buoy directions. A second test compares the f, θ spectral distance between peaks in relation to their individual spectral spreads. Peaks are combined if the spread of either peak is large compared to the distance between the two peaks. Wave component statistics are updated after each combination is made.

d. Minimum Wave Height Threshold and Storage of Results

As a final step in producing consistent results with minimal noise, any wind-sea or swell component that falls below a significant wave height threshold of 0.1 m is removed from analysis and labeled as miscellaneous energy.

The partitioning results are stored in a wave component template $T(f,\theta)$ that has the same degrees of freedom and cut-off frequency as the input spectrum. Matrix values contained in the template can be one of the following:

Matrix Value	Represents
0	Wind Sea
1…n	Swell System ID
-1	Miscellaneous energy

An example of a partitioned buoy spectrum containing a wind-sea and three swell components appears in Fig 3.

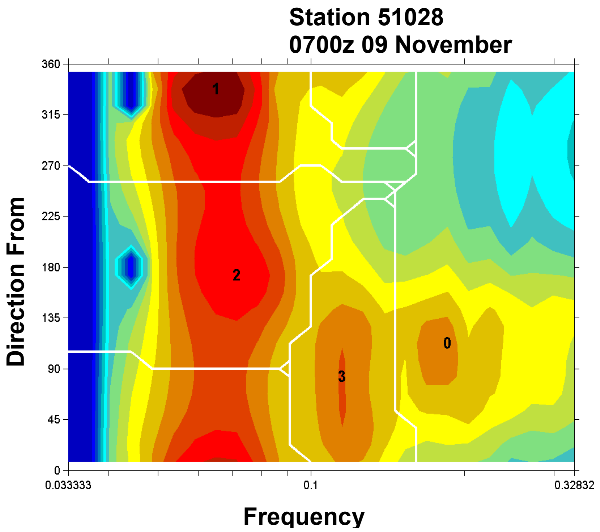

Note: Energy levels logarithmically scaled to the peak value

Fig. 3. Example partition results for buoy station 51028 2D spectrum on 9 November 2000 (0700 GMT). White lines denote the boundaries of each wave component as represented in the partition template $T(f,\theta)$. Note that this record contains a wind sea (0), North Pacific swell (1), South Pacific Swell (2), and a more locally-generated easterly swell (3).

e. Swell Tracking

Once a time series of directional wave spectra has been partitioned, a clustering algorithm is used to link common wave components together through time. This results in the generation of wave systems, which are statistically represented by time-evolving series of H_s (approximated by H_{mo}), T_p, and $\bar{\theta}$ attributes associated with each wave component. A convenient display of these features is in the form of the wave vector history plot shown in Fig 4a. At any given time, the wave field is composed of multiple wave components that are members of a distinct evolving wave system. For example, the wave vectors at the dashed vertical line in Fig 4a correspond to the wave components identified in Fig. 3. The wave vector history shows how these particular components evolve through time. Wind-seas (black arrows) are driven by local winds. The swell events are more persistent, with systems from the North and South Pacific both typically lasting about 6 days. It is interesting to note that the two most energetic wave height events during this two-week period (Fig. 4b) are a result of the superposition of locally increased wind-seas with energetic swells from three different origins.

3.2. Wave Component Module

The Wave Component Module (Fig. 2) evaluates the wave model differences from observations in the partition domains of each wind-sea and swell component. These differences are here attributed to model errors, which makes the assumption that buoy data are truth. Module inputs are the hindcast 2D spectra $S(f,\theta)$, the buoy wave partition template $T(f,\theta)$, and the associated wave component and full-spectrum statistics (H_s, T_p, $\bar{\theta}$ and σ). Each hourly hindcast spectrum is time paired to the corresponding buoy partition template for that location. An overlay of the buoy partition template on the hindcast spectrum provides a means to generate hindcast component statistics covering the same spectral (f,θ) domain represented in buoy data. As an example of this process, in Fig. 5 we overlay the buoy partition template of Fig. 3 on the corresponding hindcast spectrum. To generate a set of hindcast statistics to compare directly with the buoy statistics, The Wave Component Module then computes integral H_s, T_p, $\bar{\theta}$ and σ statistics for each buoy partition domain in the hindcast spectrum.

The buoy and hindcast component statistics are grouped into four classes: full spectrum, wind-sea, primary swell and secondary swell. Primary swell statistics represent the swell component with the largest total energy e in each record. All remaining swell partitions are treated as individual components yet grouped into the single class of secondary swell. Hindcast error metrics are computed for the H_s, T_p, $\bar{\theta}$ and σ statistics in each wave component class. For the series of buoy measurements m and hindcasts h these metrics include the means

$$\overline{m} = \frac{1}{n}\sum m$$

$$\overline{h} = \frac{1}{n}\sum h\,;$$

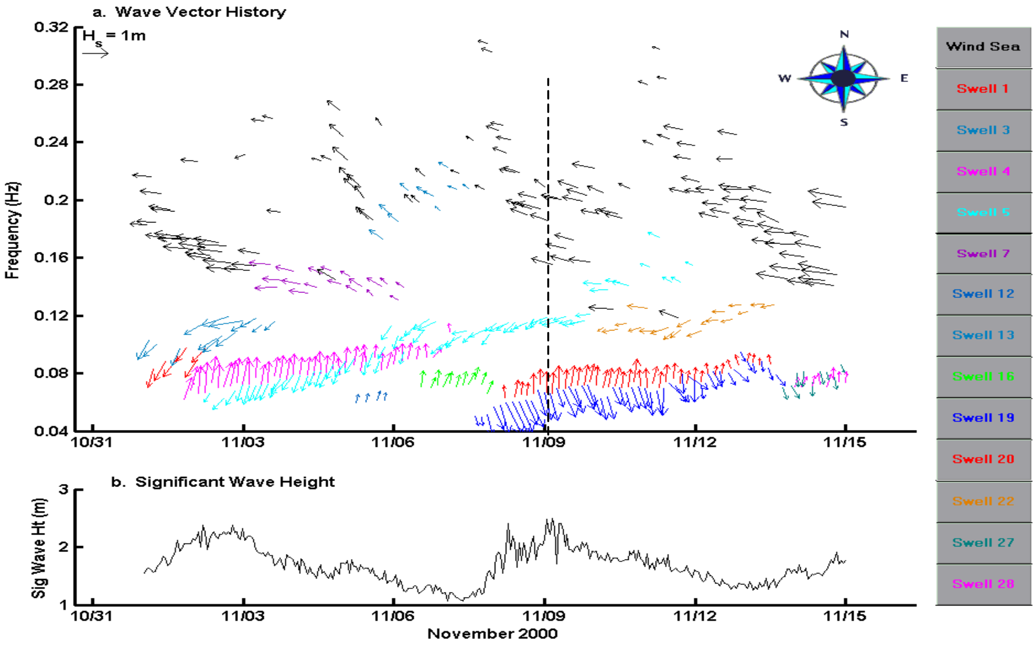

Fig. 4. Example results from Spectral Partitioning Module showing persistent wave system evolution during November 2000 at Station 51028. a. Wave vector history. Wave vectors represent the height (length), peak frequency (origin), and direction of travel (azimuth) of evolving wave systems (color-coded). For clarity, only wave systems persisting 10-h or longer are displayed. b. Full-spectrum significant wave height.

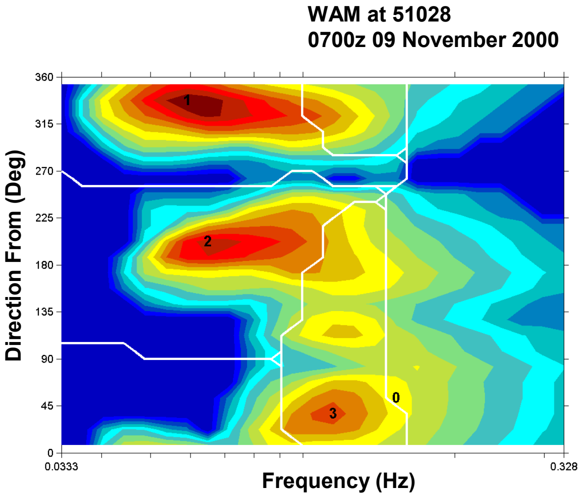

Fig. 5. Buoy partition template (from Fig. 2) over WAM hindcast 2D spectrum for 0700z, 9 November 2000 at station 51028.

bias (hindcast-buoy)

$$b = \frac{1}{n}\sum h - m\,;$$

and root-mean-square error

$$e_{rms} = \left[\frac{\sum (h-m)^2}{n}\right]^{0.5}$$

(Cardone et al. 1996). To allow investigation of seasonal trends, error statistics at each observation station are computed on a monthly basis.

3.3 Wave System Module

The Wave System Module (Fig. 2) is a tool for diagnosing sources of hindcast errors identified by the Wave Component Module. It is specifically used to access model performance in the generation and evolution of wave system energy. Inputs to the module are the time-evolving buoy and hindcast wave system statistics H_s, T_p, and $\overline{\theta}$.

As Pacific Ocean buoy stations can be subjected to dozens of wave systems over the coarse of a month (Fig. 4), the total wave power $\overline{I}$ is used to identify and select the most energetic systems for analysis (US Army Corps of Engineers, 2003). The average flux of wave energy $\overline{E}$ per unit wave crest is governed by the wave group velocity C_g such that

$$\overline{P} = \overline{E}C_g$$

where $\overline{P}$ is often referred to as the wave power per unit crest length and C_g is approximated by

$$C_g = \frac{gT_p}{4\pi}.$$

Integrating $\overline{P}$ over the duration of a particular wave system yields the integrated wave power or total intensity of a wave event per unit crest length

$$\overline{I} = \int \overline{P}dt = \int \overline{E}C_g dt = \int \frac{\rho g H_s^2}{16} C_g dt. \qquad (4)$$

Setting units of ρ(kg/m^3), g(m/s^2), H_{mo}(m), C_g(m/s) and t(s) in the above yields $\overline{I}$ in units of Joules/m. This can be interpreted as the total work done by the wave system over a crest length of 1 m. Typically the 10 most energetic wave systems in a given monthly record are selected for enhanced analysis.

For each of these observed wave systems, the hindcast wave systems are searched to find a match based on record duration, time overlap with the buoy data, mean wave period and mean wave direction. Resulting comparisons of hindcast and measured wave system statistics are displayed graphically in the form of time series. Although no quantitative metrics are currently generated, the resulting displays provide a powerful visual tool to aid in the diagnosis of model deficiencies.

4. RESULTS

A first step in executing a wave system analysis for model performance is to quantify the monthly wave component hindcast errors at each station. It is found that the WAM Pacific Ocean hindcast errors exhibit strong seasonal trends with remarkable agreement between most stations. Wind-sea and primary swell H_s hindcast errors appear in Fig. 6. Secondary swell hindcast errors follow those of the primary swell and have been omitted for clarity. Both wave components reveal reduced RMS errors in wave height from April to September with sharp increases at most stations occurring during the winter. Wind-sea height bias at all stations except 46042 is between 0 and –0.2 m in the summer months, and more strongly negative (-0.2 to –0.6 m) in winter. This contrasts sharply with swell height bias, which remains positive (0 to 0.5 m) all year long with the exception of Stations 46029 and 00071 becoming slightly negative in October. Station 51028 exhibits the strongest seasonal trend in swell height bias with 0 to 0.2 m bias in the summer months increasing to > 0.4 m in winter. There is little or no discernable geographic trend to the observed errors.

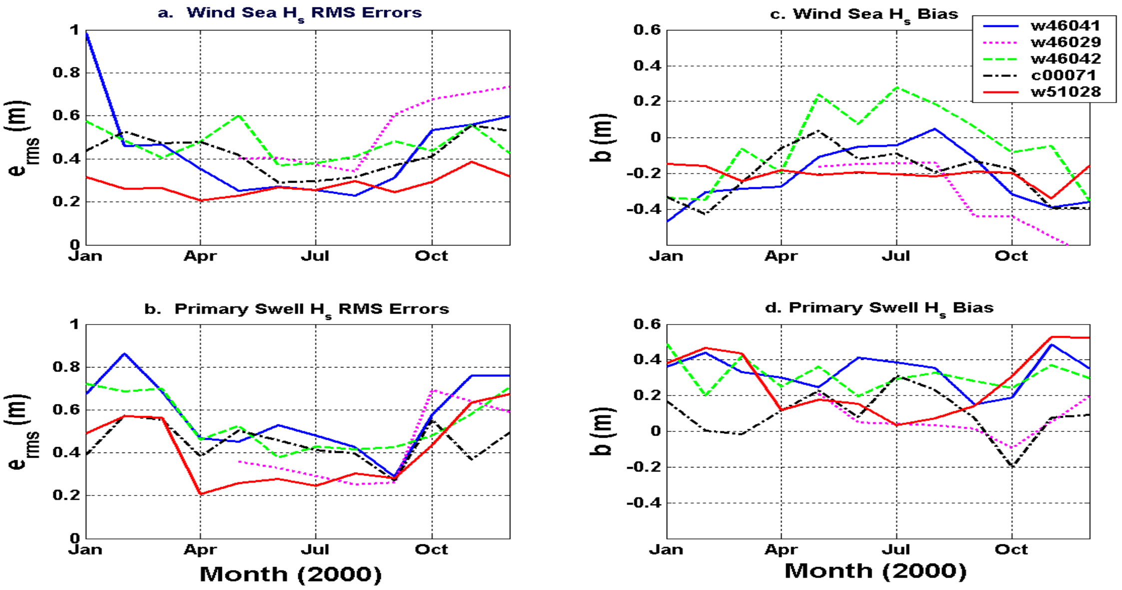

Fig. 6. Monthly wind-sea and swell significant wave height hindcast errors. a. Wind-sea *erms*. b. Primary swell *erms*. c. Wind-sea *b*. d. Primary swell *b*.

Monthly wave component peak period T_p hindcast errors appear in Fig. 7. Wind-sea and swell wave period errors are quite reasonable with a small 0- to 1-s positive bias for wind-sea periods and a –1- to 1-s bias for swell. Only the station 51028 wind sea errors hint at a seasonal trend, while all stations exhibit at least some seasonal trend in swell period. The strongest seasonal trend in swell period bias appears at the California stations 46042 and 00071, with a 0.25 to 1 s positive wave-period bias in winter contrasted with a – 0 to –1 s negative bias in summer.

The monthly mean direction $\overline{\theta}$ wave component hindcast errors are displayed in Fig. 8. Strong seasonal trends in wind-sea direction RMS errors are exhibited at all stations except 51028. Elevated wind-sea mean direction errors in winter months, with a corresponding negative wind sea bias, are a testament to stronger, more highly variable wind forcing which may not be well represented in the hindcast winds. Swell direction errors are quite low with little month-to-month variability.

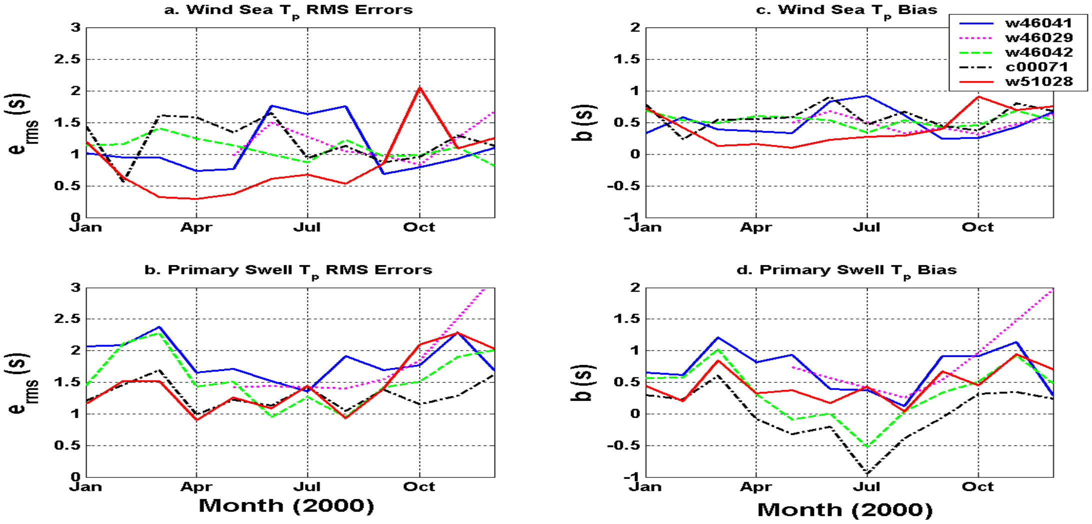

Fig. 7. Monthly wind-sea and swell peak wave period hindcast errors. a. Wind-sea *erms*. b. Primary swell *erms*. c. Wind-sea *b*. d. Primary swell *b*.

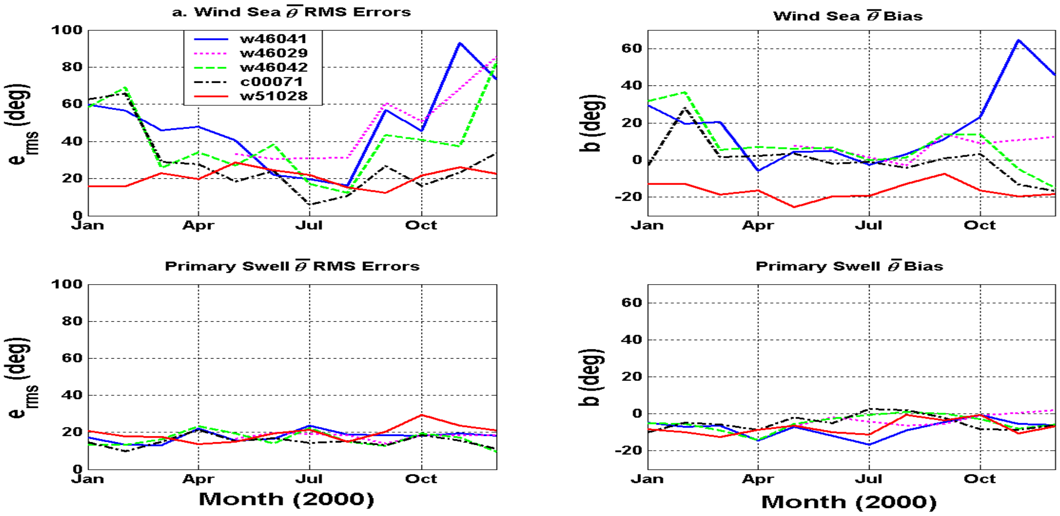

Fig. 8. Monthly wind-sea and swell mean wave direction hindcast errors. a. Wind-sea *erms*. b. Primary swell *erms*. c. Wind-sea *b*. d. Primary swell *b*.

The hindcast errors represented in Figs 6-8 provide a monthly assessment of WAM model performance at each station in replicating the measured wind-sea and swell wave components in the wave field. They identify key areas requiring further analysis to fully access deficiencies in the wave model and/or the wind fields. Perhaps the most striking finding is the disparity between wind-sea and swell height bias. How can wind-seas with too little energy result in swells with too much energy? To address this issue, station 51028 November 2000 results are examined in further detail. This station, located in an open ocean deep-water site (Table 1 and Fig. 1), is subject to a full spectrum of Pacific Ocean wavefields and can be used to gage model performance from a number of significant generation regions. The month of November was chosen to exemplify the contrast in wind-sea and swell height bias observed at essentially all stations early and late in the year.

A comparison of the station 51028 hourly November 2000 wave component hindcasts and measurements are provided by the H_s, T_p, $\overline{\theta}$ and σ scatter plots of Fig. 9. These are the data used to compute the monthly hindcast errors presented above (Figs. 6-8). The wave height results (Fig. 9a) exemplify the clear bias differences between wind-sea and swell. Note that the few hindcast wind-sea heights that fall above 1.5 m do not exhibit a negative bias. In contrast, the majority of the wave component peak period (Fig. 9b) estimates agree very well with the measurements. An exception to this is a small cluster of very long period (~20 s) hindcast estimates that over-estimate the measured wave periods by 5 to 10 s. Mean wave direction estimates (Fig. 9c) show reasonable agreement with the measured directions, with easterly wind-seas biased to the North and some northerly swells biased a bit to the west. A comparison of the hindcast and measured directional spread (Fig. 9d) exhibits two distinct data clouds. All the wind-sea spreads and a significant population of the swell spreads fall in a large data cluster with no obvious net bias yet a very high degree of scatter. In particular the hindcast spreads in this domain appear to have a much larger dynamic range than the buoy results. A second cluster of data exhibit very narrow hindcast spreads of less than 20 deg with corresponding measured values between 30 and 50 deg for the bulk of the data.

The wave component analysis presented here has provided us with a great deal of information on WAM performance in estimating particular components of the wave spectrum. Additional information on sources of these errors can only be obtained by looking at specific details of the evolving wave systems. This is accomplished in the following sections, with wind-sea and swell errors treated separately.

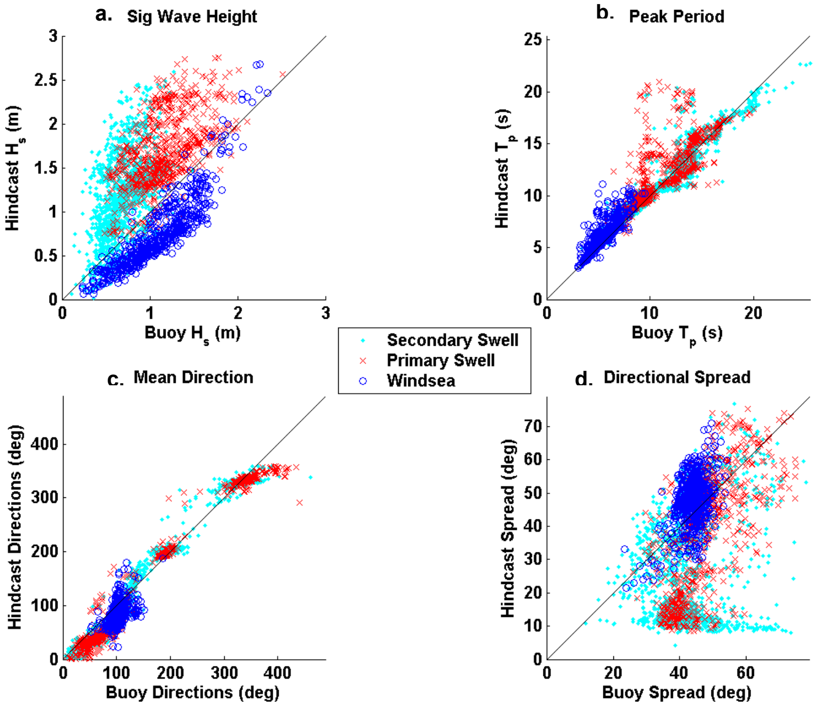

Fig. 9. Wave component observation and hindcast scatter plots from NDBC station 51028 during November 2000.

4.1 Wind-Seas

The wave component hindcast analysis has revealed a strong negative wind-sea height bias during the winter months at all five stations (Figs. 6 and 9). Although it is possible that a systematic bias in the input winds might lead to such an effect, this is unlikely due to the high degree of care expended in the preparation of the NRAQ Level III wind fields. To verify this, time series of the measured and hindcast wind speeds for station 51028 during the month of November 2000 appear in Fig. 10. Small scale (hourly) wind speed and direction fluctuations are not captured by the hindcast winds. The larger-scale (daily) fluctuations are reasonably well captured with no apparent consistent bias in magnitude. A verification of this appears in the wind speed scatter plot of Fig. 11. The hindcast data are very evenly distributed with no net bias towards either low or high winds. Examination of several additional monthly records has verified this finding to be somewhat universal. Hence it appears that we can rule out the WIS winds as the source of a persistent wind-sea bias.

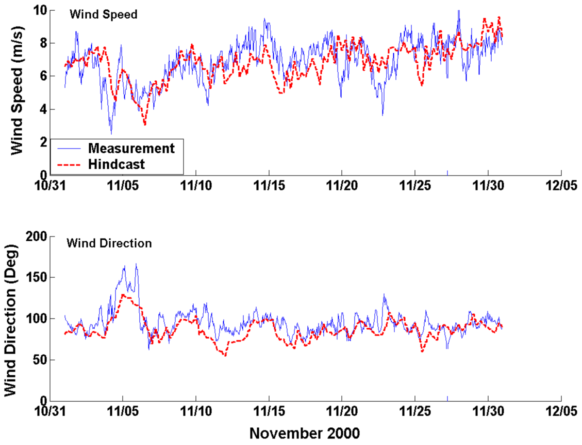

Fig. 10. Time-series comparison of November 2000 measured and hindcast wind speeds at Station 51028.

To further investigate the source of anomalously low hindcast wind-sea heights, the 1D spectra from several wind-sea episodes have been examined in detail. A consistent under-estimation of spectral levels in the equilibrium range of the spectral tail is apparent during rapidly changing wind conditions, such as are known to prevail throughout the winter months. The 1-3 November wind-sea event at station 51028 (Fig. 4) provides an excellent example of this. Wind speeds were fairly steady at 6-8 m/s from the east during this period.

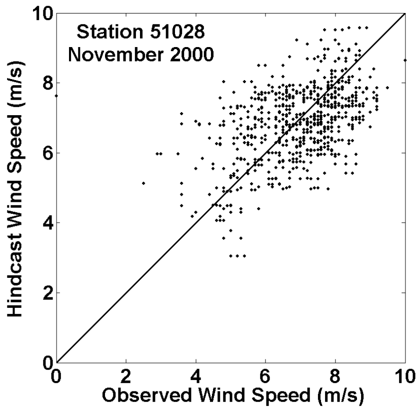

Fig. 11. Scatter plot of November 2000 measured and hindcast wind speeds at Station 51028.

A comparison of hindcast and measured 1D wave spectra from this event appear in Fig 12, along with Pierson-Moskowitz (1964) model estimates for a fully-developed wind-sea. In the growth phase of this event (Fig. 12a), a measured wind-sea peak is completely absent from the hindcast spectrum, and spectral levels in the equilibrium range of the hindcast tail are significantly lower in energy. Hindcast spectral levels increased during the final stages of this event (Fig. 12b) and ultimately matched the measured levels. However note that this was only achieved with hindcast wind speeds 1.8 m/s greater than those observed at the buoy. In general it was found that hindcast wind-seas respond too slowly to the winds and that elevated or consistently steady winds are required to match spectral levels. This result may offer an explanation for the high wind-sea direction errors typical of winter months (Fig. 8). Potential factors responsible for the observed windsea hindcast errors will be further addressed in the discussion.

4.2 Swell

The wave component error analysis revealed a positive bias in hindcast swell height at all stations during most months (Fig. 6d). Furthermore, an examination of the station 51028 hindcast swell heights during November 2000 indicates that there is a fair amount of scatter to this bias (Fig. 9a) in both primary and secondary swell components. How are these errors distributed throughout the various wave systems arriving at 51028? Do they come from a particular generating area? Are there any consistent patterns? We can use our wave systems approach (Fig. 2) to obtain additional forensics information about the manifestation of these errors within the wave hindcast.

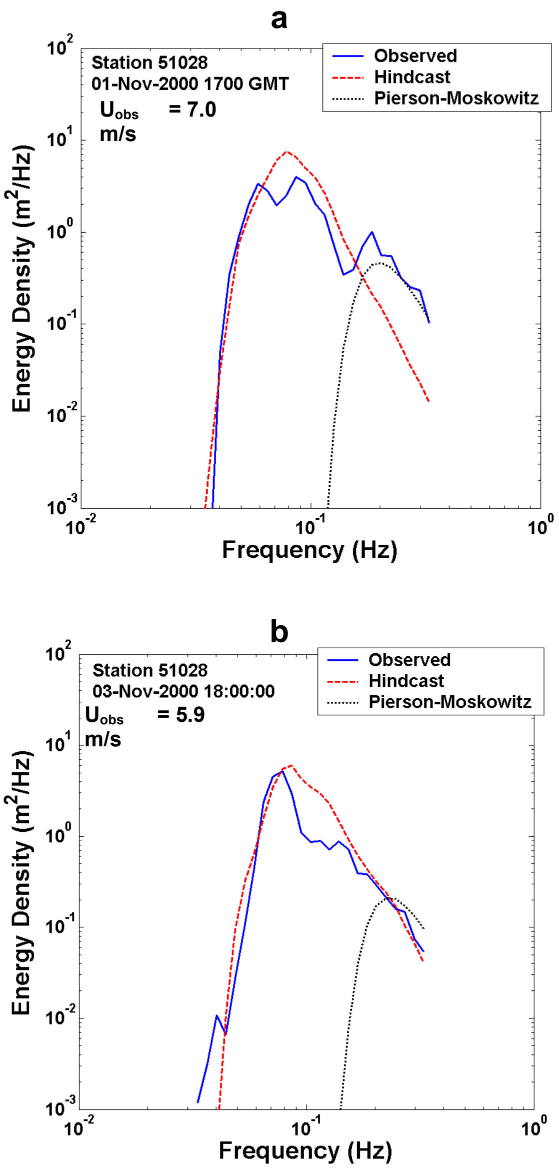

Fig. 12. Station 51028 measured and hindcast 1D wave spectra at two selected time periods during a wind-sea event: a. 1700 GMT on 1 November, and b. 1800 GMT on 3 November. A Pierson-Moskowitz model prediction for the observed wind speeds are included.

To identify the events most likely to influence a positive swell height bias, the integrated wave power (Eq. 4) was computed for each hindcast wave swell system at station 51028 during November 2000. Wave vector time series of the ten most energetic systems from the hindcast, along with their representative systems in the buoy data, appear in Fig 13. Note that WAM produces very sharply defined evolving wave fields exhibiting a smooth temporal variation in height, period and direction. The buoy wave systems appear less distinct yet there is a swell system for every major hindcast system. The results suggest a very complicated swell field, with simultaneous wave systems arriving from each of the primary generation areas (A through D) depicted in Fig. 1. The higher level of variability in the wave buoy systems can be a result of many factors; including geophysical variability in wind forcing and ocean currents, nonlinear interactions with opposing storms and associated wave fields, sampling variability and instrument noise. Allowing for these factors that are not included in WAM, the hindcast skill in depicting the evolution of each wave system is striking.

The manifestation of H_s, T_p, and $\bar{\theta}$ hindcast errors in these results can be determined through direct comparison of individual hindcast wave systems with their measured counterparts. We have found that the hindcast errors in swells have a strong dependence on generation region, with errors from a particular generating region being very similar from wave system to wave system. Example comparisons of hindcast and measured wave system H_s, T_p, and $\bar{\theta}$ statistics from each of the four major November generating areas for station 51028 (Fig. 1) appear in Figs. 14-17. The swell hindcast results from each of these generation regions are described below. The reader is referred to Fig. 1 for reference on the location of each generation region, and to Fig. 13 for the evolution of primary swell systems from each region. The reader should note that the highly variable nature of the measurement data in Figs 14-17 is not all attributed to geophysical variability. There are a number of potential noise sources including instrument related noise, sampling variability, and data processing artifacts. What is most important to look for in these figures is the agreement of the mean observed levels and trends with the hindcasts.

As Fig. 13 depicts, a 14-day series of highly variable swells arrived at station 51028 from generation region A. These are a result of the northern hemisphere northeast trade winds, which produce a belt of elevated winds across the Pacific centered at about 15 deg N Latitude. A direct comparison of the measured and hindcast features of these swells appear in Fig. 14. Mean observed wave heights are 1.2 m, with an approximate 0.3 m positive bias in hindcast heights. Hindcast wave periods and directions both show fair agreement given the high variability of the measurements.

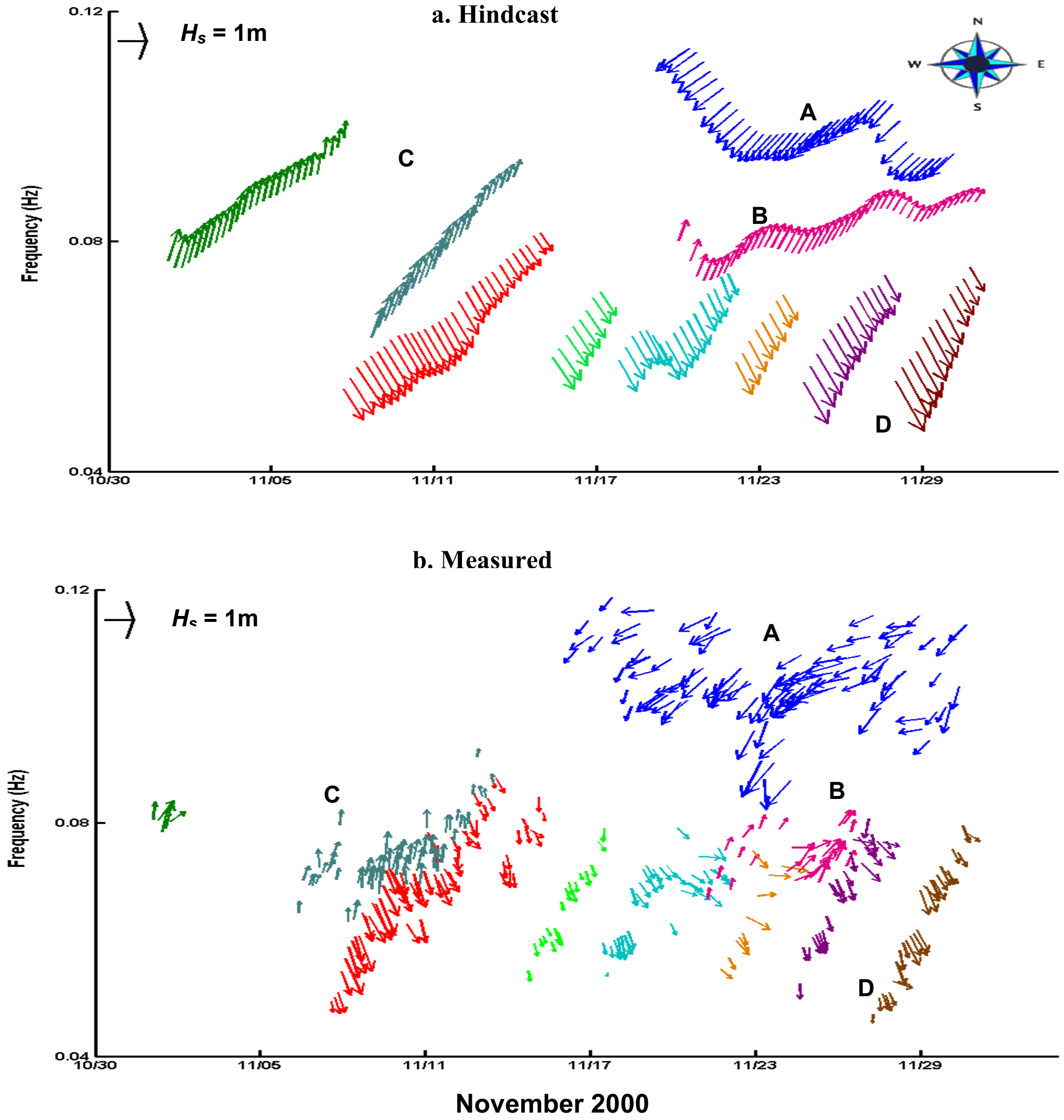

Fig. 13. Wave vector plots of ten most energetic swell systems at station 51028 during November 2000. Each hindcast wave system in (a) has a measured counterpart in (b). Lettered swell systems are associated with the wave generation areas of Fig. 1.

Generation region B is a result of mid-latitude ‘spring’ storms below the equator. These events appear to form in the Tasman sea and move easterly across the Pacific. A component of this motion directed towards the northwest results in the production of swell energy that reaches station 51028. Comparisons of measured and hindcast swell features from generation area B appear in Fig. 15, corresponding to wave vector system B in Fig. 13. Mean observed wave heights are 0.9 m. Except for a single observation at the peak of this event, hindcast wave heights are nearly continuously too high with a 0.2-m average positive bias. Hindcast wave periods have a small -1.2 s negative bias, and directions agree favorably with the measurements.

Generation area C is a result of high-latitude storms deep in the southern ocean. These fierce anti-cyclonic storms are strongest during the southern hemisphere winter months (June-Aug) and are significantly diminished by November. However, sufficient wind forcing exists to produce swells which can travel 5700 km to reach station 51028. Comparisons of measured and hindcast swell features from generation area C appear in Fig. 16. This event corresponds with the mid-frequency (teal-colored) wave vector system passing through 11 November in Fig. 13. Observed wave heights average 0.8 m, with hindcast wave heights consistently biased 0.5-m above the observations. Hindcast wave periods are in excellent agreement with the observations, and depict a strong dispersive signature typical of waves that have traveled a great distance. Hindcast directions suggest a 15-deg bias to the west.

As Fig. 13 indicates, a continual series of swell systems arrive at station 51028 from generation area D in the North Pacific (Fig. 1). These are a result of the low-pressure winter cyclones that regularly pass across the North Pacific during winter months, producing a dynamic multi-component wave field in the Gulf of Alaska (Hanson and Phillips 2001). The swells reaching station 51028 from generation region D have traveled up to 6500 km. Comparisons of measured and hindcast swell features from a single swell system originating in the North Pacific appear in Fig. 17. It corresponds with the low-frequency (brown-colored) wave vector system passing through 29 November in Fig. 13. The mean observed wave height of 0.9 m for this event is contrasted sharply by a 2.0-m mean hindcast wave height. Furthermore, hindcast wave heights are 1.8-m above the observed heights at the onset of this event. In contrast to this strong positive swell height bias, hindcast peak periods and mean directions are very good. These results are typical of all generation area D events, with a consistently high swell height bias, accurate swell periods, and reasonably accurate swell directions

Further understanding about the manifestation of hindcast errors in the spectral estimates can be obtained through examination of the directional spread (σ) of evolving wave components. As previously demonstrated in Fig. 9, the spread of station 51028 November swell components is distributed into two distinct populations, with one set of hindcast spreads significantly lower than the corresponding buoy observations. Further sorting of these data reveals that the narrow hindcast spreads (< 20 deg) are exclusively associated with wave systems evolving from the distant generation areas C and D (Fig. 1). If the buoy spreads are correct, then it appears that some spreading mechanism is absent from the WAM propagation.

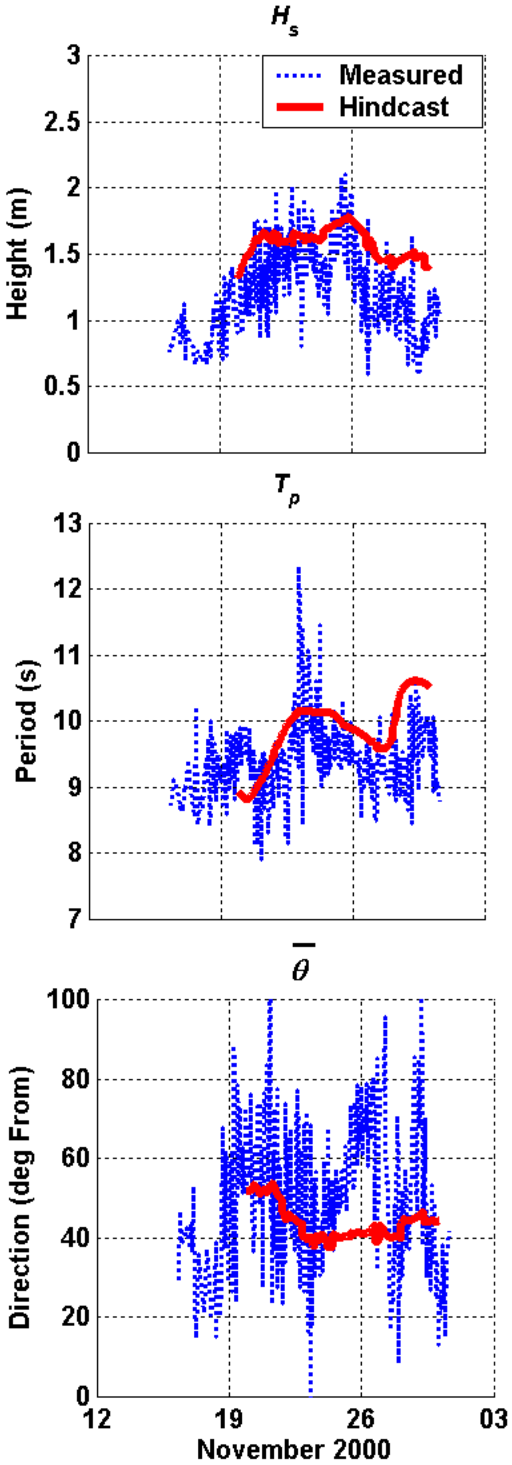

Fig. 14. Comparison of Measured and Hindcast wave system attributes from the southeast trade wind generation region A.

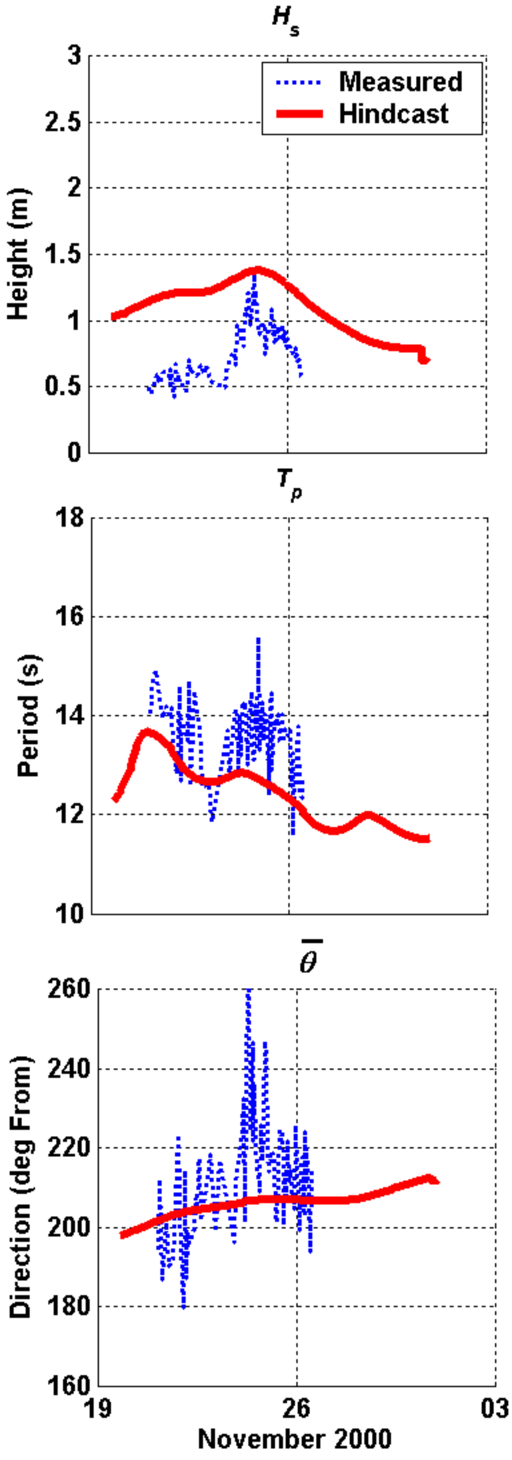

Fig. 15. Comparison of Measured and Hindcast wave system attributes from the mid-latitude southern generation region B.

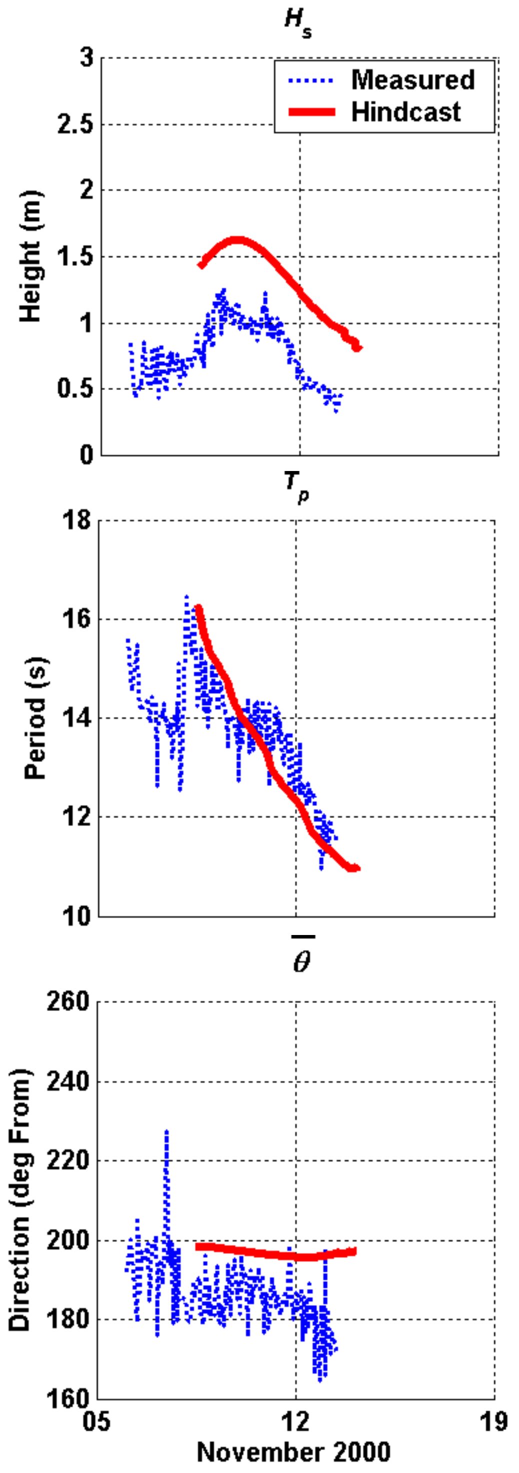

Fig. 16. Comparison of Measured and Hindcast wave system attributes from the high-latitude South Pacific generation region C.

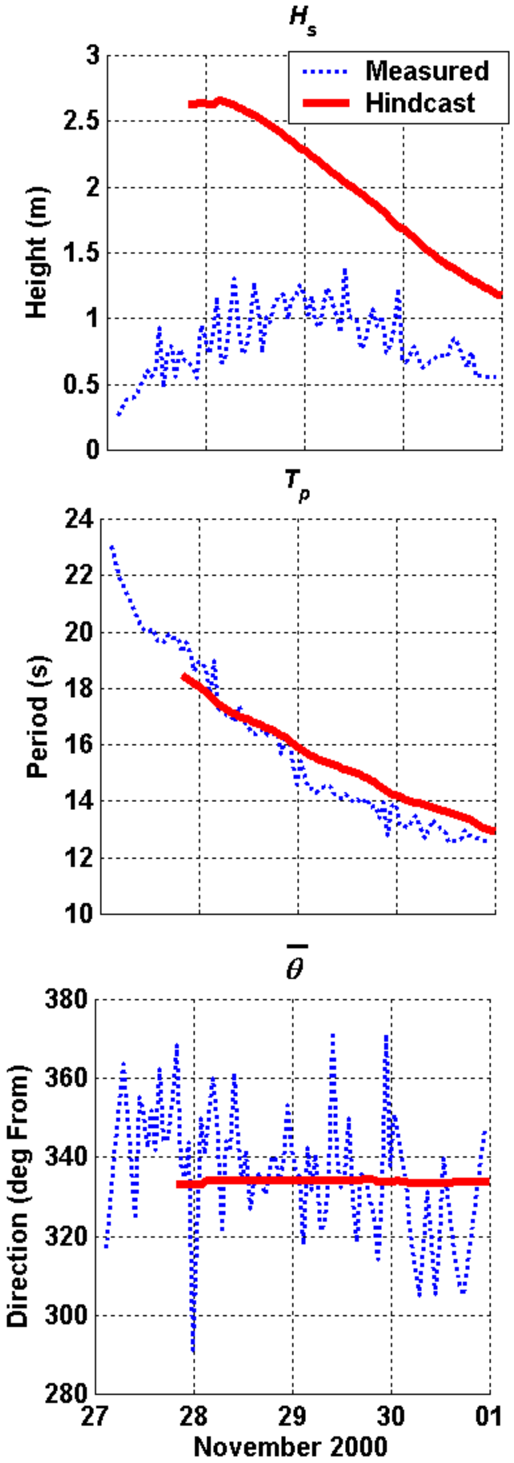

Fig. 17. Comparison of Measured and Hindcast wave system attributes from the high-latitude North Pacific generation region D.

5. DISCUSSION

The purpose of this investigation was to demonstrate a new approach for the validation and diagnostic evaluation of numerical ocean-surface wave model performance. We have shown that, when applied to a Pacific Ocean WAM hindcast, wave component and wave system analyses yield detailed information on the source of differences between observations and model estimates. In this discussion we will address the diagnostic evaluation of WAM model behavior and review limitations and alternative methods to this approach.

5.1 Wave System Diagnostics

The WAM hindcast monthly wave component errors presented in Figs. 6-8 quantify model performance in terms of the spectral representation of individual wind-sea and swell wave components. This presents a significant level of improvement over the use of bulk statistics, as the partitioning of hindcast errors between wind-sea, primary swell and secondary swell is now possible and integral period and direction metrics have meaningful interpretations. Of significant interest to this investigation are the opposing trends in wind-sea and swell height bias. As suggested by Fig. 12, the negative wind sea bias is from an apparent ‘sluggish’ response of the wave model to changing wind conditions. This may reflect an improper formalism of the wind input source term $S_{in.}$ It may also suggest an imbalance between S_{in} and the dissipation S_{ds} source terms (Eq. 3), such as improper use of S_{ds} to tune model output in terms of bulk statistics. The lower hindcast wind-sea heights may also be a result of a mismatch between the wind analysis and wind generation spatial domains. The Q-Q wind analyses are performed over large spatial domains that may smooth over smaller scales of wind variability, including mesoscale wind structures such as would lead to the hourly-scale wind fluctuations appearing in the measurements of Fig. 10. These hourly-scale fluctuations will result in local wind sea growth that is not captured by the model.

Hindcast results indicate that negative wind-sea height bias is sharply contrasted with a positive swell height bias (Fig 6). The wave system analysis reveals that the magnitude of this bias is a function of swell generation area, with larger height errors associated with those swell systems that have traveled the greatest distance (Figs 14 – 17). This may suggest a source term imbalance in wave propagation. Older swell events exhibit very close agreement of hindcast and measured swell periods, suggesting that the initial wave development at the source was correct. However the close agreement of wave period is also strongly modulated by wave dispersion along the propagation path. It should also be noted that the farthest generation areas from station 51028 have the highest wind speeds. Although not directly supported by the negative wind-sea bias, this may also suggest that S_{in} be revisited. Another factor that may contribute to excess swell energy is the grid resolution. Numerous islands in the western tropical Pacific that effectively block swell energy may be too small to be adequately represented in the 1-deg resolution of our hindcast grid. Inspection of swell energy levels in the 1D buoys to the north of Hawaii would help resolve this issue, as the North Pacific swell paths to these locations are not blocked by small islands.

5.2 Limitations and Suggested Improvements

The primary limitation to the wave system validation and diagnostics approach is a severe lack of ground truth data. The number of operational directional wave stations is to small to allow a comprehensive verification of model output. The primary benefit of these tools in their present form is to provide an augmentation of traditional bulk validation techniques.

Additional sources of information can be incorporated to make this approach more operationally viable. For example, extension of the partitioning approach to the 1D spectral domain would add several stations of available ground-truth information. Although directional statistics would not be available, it is feasible that the heights and periods of 1D wave components could be isolated and compared to corresponding hindcast values at these stations. While wave components from different generation regions could be lumped into similar categories, the analysis would provide an enhanced level of diagnostics information above pure bulk statistics. An additional potential source of ground-truth information would be from satellite Synthetic Aperture Radar (SAR) measurements (Beal et al., 1989). Estimates of ocean surface directional wave spectra, obtained along the SAR track, could be used to validate the spatial representation of evolving hindcast wave systems. However, SAR observations are not presently available for routine operational use in the United States. In the absence of SAR, significant wave height estimates from satellite altimeters can be used to verify the spatial distribution of bulk hindcast wave heights.

There are limitations to the partition template overlay method used to match up observed and hindcast wave components. As demonstrated by Fig. 3, the partition template distinctly maps out the spectral domain of each observed peak. However, portions of the energy from multiple hindcast peaks may fall into one of these domains, such as is demonstrated by swell system 3 in Fig. 5. Hence, the calculation of hindcast wave height, period and direction in this partition will be a combined result of all the energy in the domain. This can be considered reasonable, as the error statistics reflect the problems with the model within the domain of the observed wave component. An alternative approach would be to compute a separate partition template for each hindcast spectrum, and use an objective clustering approach to match components. This would provide added benefits, such as a separate accounting of extraneous wave peaks present in either the observations or the hindcast yet absent from the other. Furthermore, as swell bias was found to be partially dependant upon swell origin, an alternative to the separation of hindcast errors by primary and secondary swell components would be to sort component errors into geographically based bins based on swell source. An additional improvement would be quantification of wave system match-up errors, such as can be computed from duration, height, period and direction attributes. These additional metrics would provide an additional measure of hindcast performance and further aid in the identification of model problems.

6. SUMMARY AND CONCLUSIONS

Standard procedures for validating numerical wave models with bulk integral statistics may generate desirable error tolerances yet mask the hindcast performance in replicating the detailed nature of an intricate wave field composed of several wave components from a variety of local, regional and distant generation areas. We have shown that a wave systems validation approach provides significantly improved measures of model performance and meaningful diagnostic clues on key model deficiencies.

The demonstration of wave system validation methods on a Pacific Ocean 1-year WAM hindcast has revealed under-estimated wind-sea heights during winter months and over-estimated swell heights that are geographically dependant upon the wave generation region. The spectral manifestation of these hindcast errors suggests specific areas for additional study including model grid resolution and numerical source term balances. The quantification and synthesis of wave system results from multiple stations will only serve to provide additional diagnostic detail on model performance.

Several improvements to the method have been discussed, including an alternative wave component match-up algorithm and component error sorting based on generation region. Our goal is to develop a robust set wave model benchmarking and diagnostics tools for the routine verification of wave model output at the wave system level. We believe that such a diagnostics capability is critical to the continued improvement and application of numerical spectral ocean wave models used for the protection of human life and property.

ACKNOWLEDGEMENTS

The authors are grateful to Dr. Donald T. Resio for several insightful suggestions and to Dr. Charles E. Long for his careful review of this manuscript.

REFERENCES

Beal, R. C., Ed, 1989: *Directional Ocean Wave Spectra*. The Johns Hopkins University Press, Baltimore, MD, 218 pp.

Cardone, V. J., R. E. Jensen, D. T. Resio, V. R. Swail, and A. T. Cox, 1996: Evaluation of contemporary ocean wave models in rare extreme events: the "Halloween Storm" of October 1991 and the "Storm of the Century" of March 1993. *J. Atmos. Oceanic. Technol.*, **13**, 198-230.

Cardone, V. J., H. C. Graber, R. E. Jensen, S. Hasselmann and M. J. Caruso, 1995: In search of the true surface wind field during SWADE IOP-1: Ocean wave modeling perspective. *The Global Atmosphere-Ocean System*, **3**, 107-150

Cox, A. T., V. J. Cardone, and V.R. Swail, 1996: An interactive objective kinematic analysis system. *Proc. 4th International workshop on Wave Hindcasting and Forecasting*, November 6-10, 2000, Monterey, CA.

Gerling, T. W., 1992: Partitioning sequences and arrays of directional ocean wave spectra into component wave systems. *J. Atmos. Oceanic Technol.*, **9**, 444-458.

Hanson, J. L., 1996: Wind sea growth and swell evolution in the Gulf of Alaska. Ph.D. Dissertation, the Johns Hopkins University, 151 pp.

Hanson, J. L., and O. M. Phillips, 2001: Automated analysis of ocean surface directional wave spectra. *J. Atmos. Oceanic. Technol.*, **18**, 277-293.

Hanson, J. L., and O. M. Phillips, 1999: Wind sea growth and dissipation in the open ocean. *J. Phys. Oceanogr*, **29**, 1633-1648.

Hasselmann, S., K. Hasselmann, and C. Bruning, 1994: Extraction of wave spectra from SAR image spectra. *Dynamics and Modelling of Ocean Waves*, G.J. Komen et al., Eds., Cambridge University Press, 391-401.

Hsu, L. Y., W. E. Rogers and J. D. Dykes, 2002: WAM performance in the Gulf of Mexico with COAMPS wind. *7th International Workshop on Wave Hindcasting and Forecasting*, Meteorological Service of Canada, 151-159.

Jensen, R. E., P. A. Wittman, and J. D. Dykes, 2002: Global and regional wave modeling activities. *Oceanography*, 15(1), 57-66.

Kalnay, E., and Coauthors, 1996: The NCEP/NCAR 40-year reanalysis project. *Bull. Amer. Meteor. Soc.*, **77**, 437-471.

Komen, G. J., L. Cavaleri, M. Donelan, K. Hasselman, S. Hasselmann and P. A. E. M. Janssen, 1994: Dynamics and Modeling of Ocean Waves. Cambridge University Press, 532pp.

O'Reilly, W. C., T. H. C. Herbers, R. J. Seymour and R. T. Guza, 1996: A comparison of directional buoy and fixed platform measurements of Pacific swell. *J. Atmos. Oceanic. Technol.*, **13**, 231-238.

Oltman-Shay, J. & R. T. Guza, 1984: A Data-Adaptive Ocean Wave Directional Spectrum Estimator for Pitch and Roll Type Measurements. *J. Phys. Oceanog.*, 14, 1800-1810.

Pierson, W.J., and L. Moskowitz, 1964: A proposed spectral form for fully developed wind seas based on the similarity theory of S.A. Kitaigorodskii. *J. Geophys. Res.*, **69**(24), 5181-5190.

Scott, D., D. Resio and C. Pantoja, 2002: Swell propagation and nearshore wave climate. *7th International Workshop on Wave Hindcasting and Forecasting*, Meteorological Service of Canada, 13-24.

Steele, K. E., C. C. Teng, and D. W. C. Wang, 1992: Wave direction measurements using pitch-roll buoys. *Ocean Eng.*, **19**(4), 349-375.

Soille, P., 1999: Morphological Image Analysis: Principles and Applications. Springer-Verlag, 170-171.

Swail, V. R. and A. T. Cox, 2000: On the use of NCEP-NCAR reanalysis surface marine wind fields for a long-term North Atlantic wave Hindcast. *J. Atmospheric Oceanic Technology,* **17**, 532-545.

Tolman, H. L., 2002: The 2002 Release of WAVEWATCH III. *7th International Workshop on Wave Hindcasting and Forecasting*, Meteorological Service of Canada, 188-197.

Tracy, B. A , Jensen, R. E. and A. Cialone, (in preparation): WIS Atlantic and Gulf Wave Hindcasts for 1980 – 1999.

US Army Corps of Engineers, 2003: Coastal Engineering Manual. Publication Number EM 1110-2-1100, Washington, DC.

Vincent, L., and P. Soille, 1991: Watersheds in digital spaces: An efficient algorithm based on immersion simulations. *IEEE Transactions of Pattern Analysis and Machine Intelligence*, **13**(*6*), 583-598.

Voorrips, A. C., V. K. Makin and S. Hasselmann, 1997: Assimilation of wave spectra from pitch-and-roll buoys in a North Sea wave model. *J. Geophys. Res*. 102, 5829-5849.